Petroleum Science 19 (2022) 2981–2994

Contents lists available at ScienceDirect

Petroleum Science

journal homepage: www.keaipublishing.com/en/journals/petroleum-science

Original Paper

Experimental study of the critical sand starting velocity of gas-water-sand flow in an inclined pipe

Rui-Yao Zhang [a], Jun Li [a, b, *], Hong-Wei Yang [a], Geng Zhang [a], Xi-Ning Hao [c], Peng-Lin Liu [a]

[a] *School of Petroleum Engineering, China University of Petroleum (Beijing), Beijing, 102200, China*
[b] *School of Petroleum Engineering, China University of Petroleum (Beijing), Karamay, 834000, Xinjiang, China*
[c] *CNOOC Research Institute Co. Ltd., Beijing, 100028, China*

A R T I C L E I N F O

Article history:
Received 9 November 2021
Received in revised form
5 September 2022
Accepted 10 September 2022
Available online 15 September 2022

Edited by Yan-Hua Sun

Keywords:
Three-phase flow
Critical sand starting velocity
Flow pattern
Sand migration
Gas void fraction
Hole deviation angles
Sand concentration

A B S T R A C T

The purpose of this paper is to study the critical sand starting velocity and transformation law of flow pattern based on gas–water–sand three-phase flow in an inclined pipe. Firstly, the indoor simulation experiment system of gas–water–sand three-phase flow was used to test the conversion law of flow pattern based upon the different gas void fraction. Secondly, the influence of slug bubbles on sand migration was investigated according to distinctive hole deviation angles, gas void fraction and sand concentration. Finally, the critical sand starting velocity was tested based on dissimilar hole deviation angles, gas void fraction, sand concentration and sand particle size, and then the influence of the above-mentioned key parameters on the sand starting velocity was debated based on the force analysis of the sand particles. The experimental results illustrated that when the gas void fraction was less than 5%, it was bubbly flow. When it increased from 5% to 30%, the bubbly flow and slug flow coexisted. When it was between 30% and 50%, the slug flow and agitated flow coexisted. When it reached 50%, it was agitated flow. Providing that the hole deviation angle was 90°, the phenomenon of overall migration and wave-like migration on the surface of sand bed was observed. On the contrary, the phenomenon of rolling and jumping migration was recognized. The critical sand starting velocity was positively correlated with the hole deviation angle and sand particle size, but negatively associated with the gas void fraction and sand concentration. This research can provide a certain reference for sand-starting production in the field of petroleum engineering.

1. Introduction

Due to weak cementation, easy collapse and narrow safety density window of shallow layers in deep water, in order to develop gas hydrate resources more efficiently in deep water, a new dual-gradient drilling technology base on double-layer pipe equipped with simpler equipment and lower cost is innovatively proposed (Khan and May 2016; Li et al., 2020; Xin et al., 2020). When this new technology is applied for natural gas hydrate production, the hydrate particles will generate phase change as the variation of wellbore temperature and pressure during the return process (Bhandari et al., 2015; Lin et al., 2013; Sun et al., 2018). Subsequently, a gas–liquid–solid three-phase flow will form in the inner pipe of the double-layer pipe. If the gas hydrate initiates a phase transition, hydrate particles of different sizes appear in the wellbore (Chen et al., 2012; Ma et al., 2014; Wang et al., 2019). The successful migration of particles to the surface ground plays a crucial role in the success of hydrate extraction process. Therefore, it is necessary to carry out relevant indoor simulation experiments to study the particle migration and the flow laws of multiphase flow in inner pipe based on the double-layer pipe.

As shown in Fig. 1, the principle of this new drilling technology is to replace the traditional drilling pipe by a double-layer one (including a outer pipe and a inner pipe). What's more, a lift pump is installed on the drill pipe close to the drill bit. Firstly, the drilling fluid is injected into the annulus between inner and outer drill pipe. Secondly, the drilling fluid mixing with the hydrate particles near the downhole enters the annulus between the outer pipe and the borehole. When the mixture reaches the lift pump inlet, they will

* Corresponding author. School of Petroleum Engineering, China University of Petroleum (Beijing), Beijing, 102200, China.
E-mail address: lijun446@vip.163.com (J. Li).

https://doi.org/10.1016/j.petsci.2022.09.004

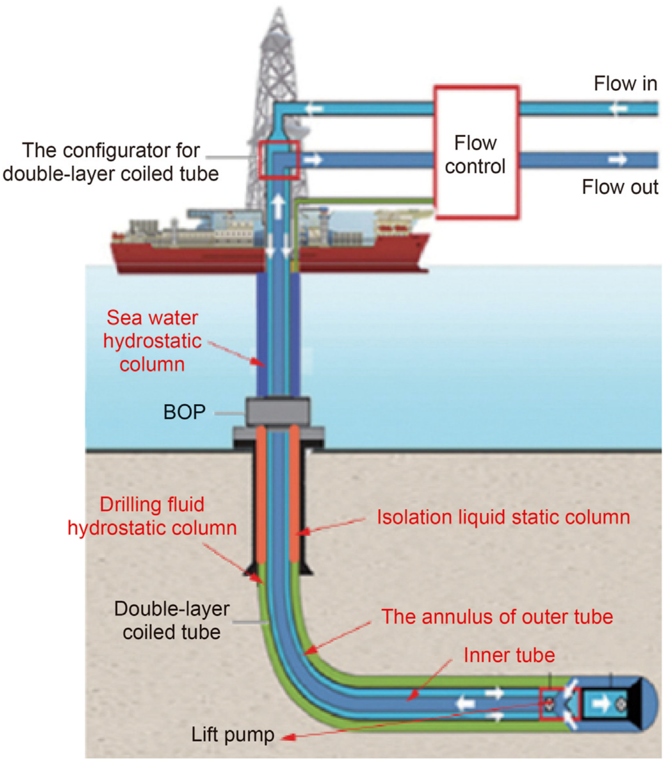

Fig. 1. Schematic diagram of dual-gradient drilling system with a double-layer pipe.

be sucked into the inner pipe due to the negative pressure generated at the inlet of the lift pump and then return to the ground. Meanwhile, the pressure difference can be adjusted by changing the pump rate to realize the control of the wellbore pressure. As the static column of low-density fluid is in the upper annulus above the lift pump, while the high-density fluid is in the lower annulus. It is called dual-gradient drilling technology based on double-layer pipe.

The natural gas hydrate will alter from the solid particle to the gas state while the wellbore temperature and pressure meet the requirements. At this moment, a three-phase flow of gas, water and sand will form in the inner pipe. However, whether the sand can migrate successfully or not will directly determine the safety and efficiency of drilling and production (GhasemiKafrudi and Hashemabadi, 2016; Elgaddafi et al., 2012; Guo et al., 2010; Mutahar, 2006; Davies, 1987). Therefore, it is necessary to perform the experimental research on the sand migration rule based on gas–water–sand three-phase flow.

Many scholars have carried out related studies of the sand migration at present. Scott and Rao (1971) gave the definition of the critical sand starting velocity in the horizontal tube by the experiment of gas–liquid–solid three-phase flow. It was the flow velocity when sand particles didn't deposit in the pipe. Shen et al. (1999) separately established the model of the critical sand starting velocity by calculating the relationship between the minimum water velocity of critical sand starting of millimeter-level solid particles in the vertical pipe. Zhang et al. (2001) ignored the Basset force and Saffman force, and only considered the gravity and buoyancy of solid particles to calculate the water velocity of critical sand starting. Li (2000) conducted the experiment of sand starting based on the single-phase liquid and solid–liquid two-phase flow in a vertical tube. The experimental results shed light on that when the water velocity exceeded 2.9 times as much as the final settlement velocity of the solid particles, the effective migration of the solid particles can be achieved. Stevenson and Thorpe (2003) investigated sand starting process of the three-phase flow of gas, water and sand in the horizontal or near-horizontal pipe. Under the low sand concentration condition, the mathematical models of critical sand starting velocity was established according to state of the intermittent and laminar flow. Keskin and Zhang (2007) carried out large quantity of experiments to gain the different empirical relationships of critical sand starting velocity based on the experimental results. Gillies et al. (1997) and Goharzadeh and Rodgers (2009) investigated the influence of gas void fraction and flow pattern on sand migration based on the experiment of gas–water–sand three-phase flow in horizontal pipe. The final results clarified that gas void fraction made little effect on sand migration, however, the opposite effect was produced by the plug flow. Liu and Deng (2007) and Jiao et al. (2010) mainly employed laboratory experiments of solid–liquid two-phase flow to have a good knowledge of the sand migration at different inclination angles. The results showed that the capacity of sand starting was the weakest when the inclined angle was at 60°, and was the best at 90°. Zhang (2013) regarded the gas-water two phases as a pseudo-homogeneous phase to establish the mathematical equation of the critical sand starting velocity for the water-bearing gas wells and obtained the variation rule of critical sand starting velocity. Dong et al. (2007, 2014) mainly studied the sedimentation of solid particles in still water and moving water to establish mathematical relationship between the sand starting velocity and the final-settlement velocity. Dabirian et al. (2016), Bello and Oyeneyin (2016), and Sui et al. (2016) separately investigated the critical flow velocity taking into account the impact of the sedimentation or sand migration based upon the gas-liquid two phase flow, solid–liquid two-phase flow and the three-phase flow of oil-water-sand.

In summary, the current research mainly focuses on the study of a single factor or two factors. It is necessary to conduct the experiment of gas–water–sand three-phase flow to better know the rule of sand migration and flow pattern transformation based on multiple factors, such as the hole deviation angle, gas void fraction, sand concentration and sand particle size. The conclusions can provide important technical reference for hydrate exploitation in dual-gradient drilling based on double-layer pipe.

2. Critical sand start-up speed experiment

2.1. Experimental system

From the above description, the hydrate particles in the inner tube will change from solid phase to gas phase while the wellbore temperature and pressure meet the requirement. The hydrate particles of different sizes, gas and drilling fluid form a multiphase flow of gas–water–sand in the inner pipe. Therefore, the object of this experiment is to simulate the migration state of hydrate particles in multiphase flow. Due to the limitation of experimental conditions, it is difficult to simulate the real wellbore temperature and pressure for the phase transition of natural gas hydrate. Hence, three different sizes of sand particles were used to represent hydrate particles with different degrees of decomposition in this experiment.

The experimental system mainly consists of several key components, such as the experimental bench, test tube, mud pump, automatic sander, air compressor, high pressure gas tank, mud pool, flow meter, high-speed camera, center console (including control cabinet), circulating pipelines, valves, etc. The part of the experimental equipment is shown in Fig. 2.

The transparent test tube was installed coaxially with the test bench, as shown in Fig. 2a. By lifting and lowering the left side of

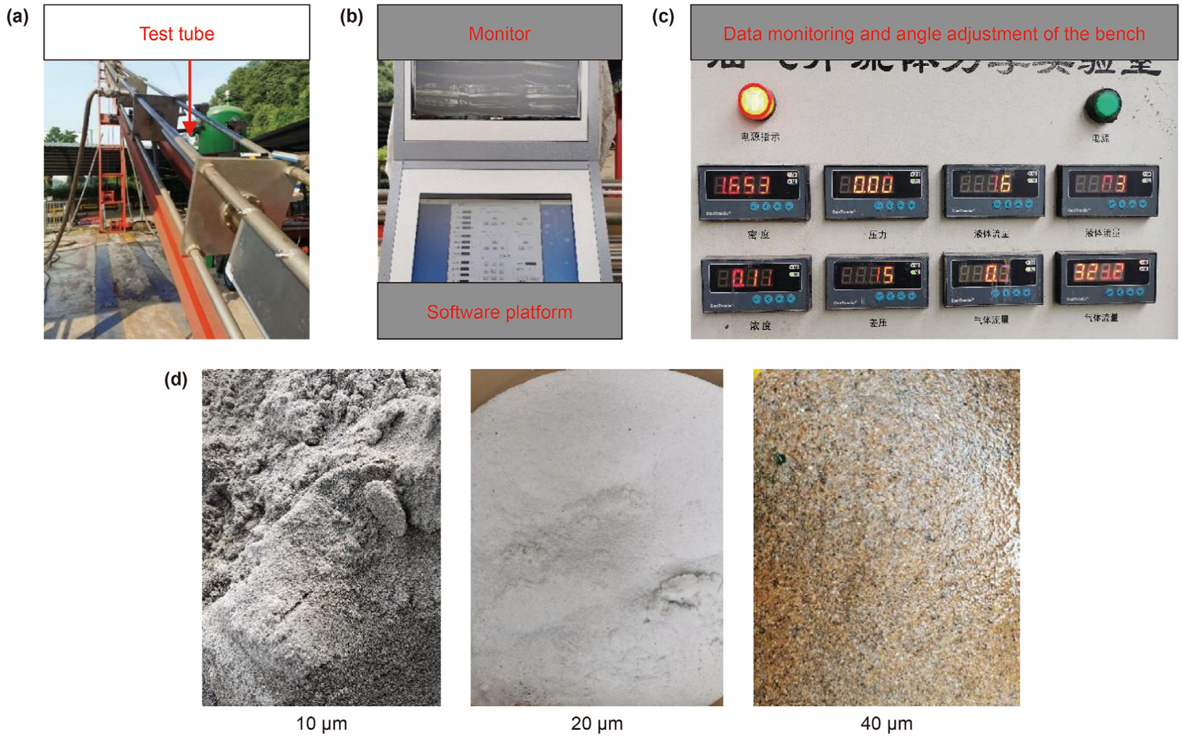

Fig. 2. The experimental system (experimental bench (**a**), center console (**b**), and control cabinet (**c**)) and sand grains of different sizes (**d**).

the test bench, the inclination of test tube can be adjusted from 0° to 90°. The main function of the center console in Fig. 2b is to control and monitor the gas flow rate, liquid flow rate, and sanding rate. Besides, it can also be applied to monitor real-time flow status in the test tube. The control cabinet in Fig. 2c is used to adjust the inclination angle of the test tube, capture the flow rate of the injected liquid and gas and then transmit them to the center console. In Fig. 2d, it is the sand particle of different sizes (average diameter). Among them, the composition of sand particles with a diameter of 10, 20, and 40 μm is the argillaceous silt or quartz silt separately.

2.2. Experimental parameters and procedures

Fig. 3 shows the sketch of experimental system. Table 1 lists the experimental test parameters and the performance parameters of the experimental equipment. The specific experimental procedures are as follows:

(1) After checking the normal operation of all instruments, turn on control and monitoring equipment and air compressors in turn.
(2) Use the control cabinet to adjust the experimental test pipeline to the predetermined angle, then open the valves 1, 2, 4, and 5 in turn, and further start up the pump with the small flow rate to clean the circulation pipe.
(3) The automatic sand and gas injection rates are calculated based on the concentration ratio of the sand and gas set by the experimental parameter, then turn on the valves 3 and 4 and set the parameter of concentration ratio through the control cabinet.
(4) When the three phases of the gas, liquid and sand in the test tube are observed to reach a relatively stable flow state, the openness of the valve 1 or 2 is reduced, so that the gravel gradually returns to the static state.
(5) Gradually turn on the openness of valve 1 or 2, so that the traffic in the test pipeline gradually increases. At this time, the motion of gravel is observed by monitoring the system. When the gravel is transformed from the original static state to the stable migration state in the direction of the fluid flow, the liquid flow rate recorded at this time is the critical flow rate for start velocity of the sand.
(6) The center console is used to adjust the injection rate of sand, the liquid flow rate while keeps the gas void fraction constant. When the ratio of the above three phase reaches the predetermined value, repeat steps (4) and (5), the critical sand starting velocity can be obtained under different sand concentration conditions. In the same way, maintain a certain sand concentration unchanged, measure the critical flow rate under different gas void fraction conditions.
(7) After the test of one certain diameter size is completed, the control cabinet is used to turn off the automatic sanding equipment and air compressor, and then start up the pump to clean the circulating pipeline.
(8) After the circulating pipeline is cleaned, repeat the experimental steps (5) and (6) to test the critical flow rate of the liquid under different gas void fraction or sand concentration based on the different diameter of the sand.
(9) When the critical flow rate of the liquid at a certain deviation angle is tested, the angle is set to the other hole deviation angle by the control cabinet. Then repeat steps (5)–(8) to critical flow rate of the liquid under the condition of different diameter of the gravel.
(10) When the parameters are completely tested, turn off the automatic sanding equipment and air compressor, and then turn on the pump to circulate the experimental pipeline. After the pipeline is cleaned, stop the pump and turn off all instruments and power supply.

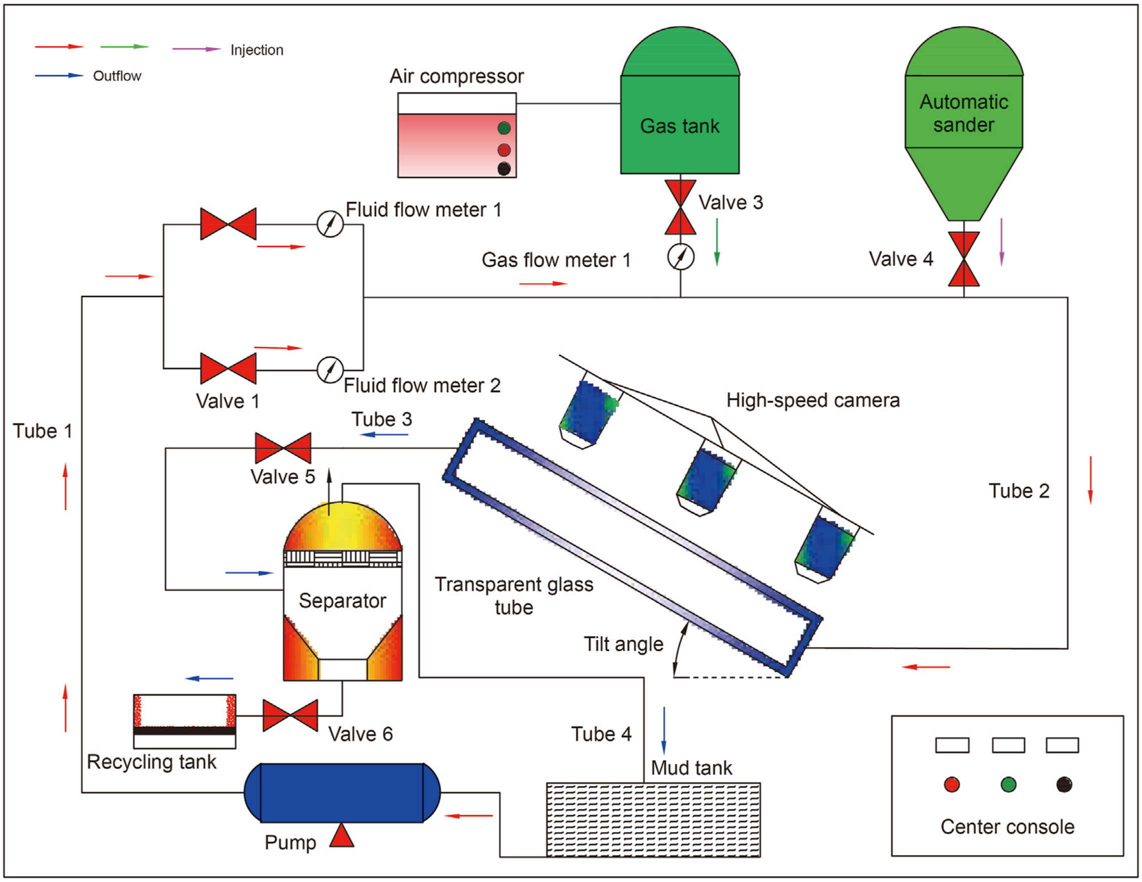

Fig. 3. Sketch of experimental system.

Table 1
Experimental parameters.

Parameter	Value
Hole deviation angle, degree	30, 60, 70, 80, 85, 90
Sand concentration, %	1, 5, 10, 30, 50
Gas void fraction, %	5, 10, 20, 30, 50
Sand diameter, μm	10, 20, 40
Pump rate, L/s	0–30
Injection speed of sand particle, kg/s	0–30
Flow rate of air compressor, m^3/min	0–32.5
Length of the test pipe, m	6
Inner diameter of the test pipe, mm	100
Angle range of the test pipe, degree	0–90

3. Experimental results

3.1. Conversion of flow pattern

3.1.1. Flow pattern at the hole deviation angle of 90°

In Fig. 4a, the gas void fraction gradually increased from zero to 5%, the flow pattern was mainly bubbly flow. When the gas void fraction steadily elevated from 5% to 10%, the critical starting velocity was altered from 0.26 to 0.21 m/s. The flow pattern progressively transited from bubbly flow to a coexistence state including bubbly flow and small slug flow. What's more, there was an obvious stratified flow state of gas, water, and sand as shown in Fig. 4b.

In Fig. 4c, the gas void fraction was further raised to 30%, there was the obvious stratified flow. But the cross-sectional width and length of the slug gradually expanded. The critical starting velocity was changed from 0.21 to 0.17 m/s. When the gas void fraction was further improved close to 50%, the flow pattern was coexistence state of local agitated flow and large slug flow, which also represented the state of transition from slug flow to agitated flow. When the gas void fraction reached 50%, the pulsating effect of the liquid increased obviously. In Fig. 4d, the liquid flew forward in a “wave-like” shape, and the flow pattern was transformed as the agitated flow.

3.1.2. Flow pattern at the hole deviation angle of 60°

In Fig. 5a, the gas void fraction was 5%, the flow pattern in the tube was mainly bubbly flow, the critical starting velocity was 0.28 m/s. As the gas void fraction gradually improved 20%, in Fig. 5b, there was no stratified flow. However, the flow pattern transited from bubbly flow to a coexistence state including the bubbly flow and small slug flow. the critical sand starting velocity was changed from 0.28 to 0.25 m/s.

In Fig. 5c, the gas void fraction was 30%, the length of the slug bubble and the cross-sectional width enlarged, the critical starting velocity reduced from 0.25 to 0.21 m/s. If the gas void fraction reached close to 40%, the sand particles rolled and jumped intensely. It was the coexistence state of the local agitated flow and large slug flow. Providing that the gas void fraction was more than 40%, the pulsating effect was more significant. Besides, in Fig. 5d, the liquid flew upward in a “spiral” shape, the sand rolled and jumped, and the flow pattern was agitated flow at this time.

It can be found that the concentration or the size of sand particles exerted little effect on the flow pattern through the

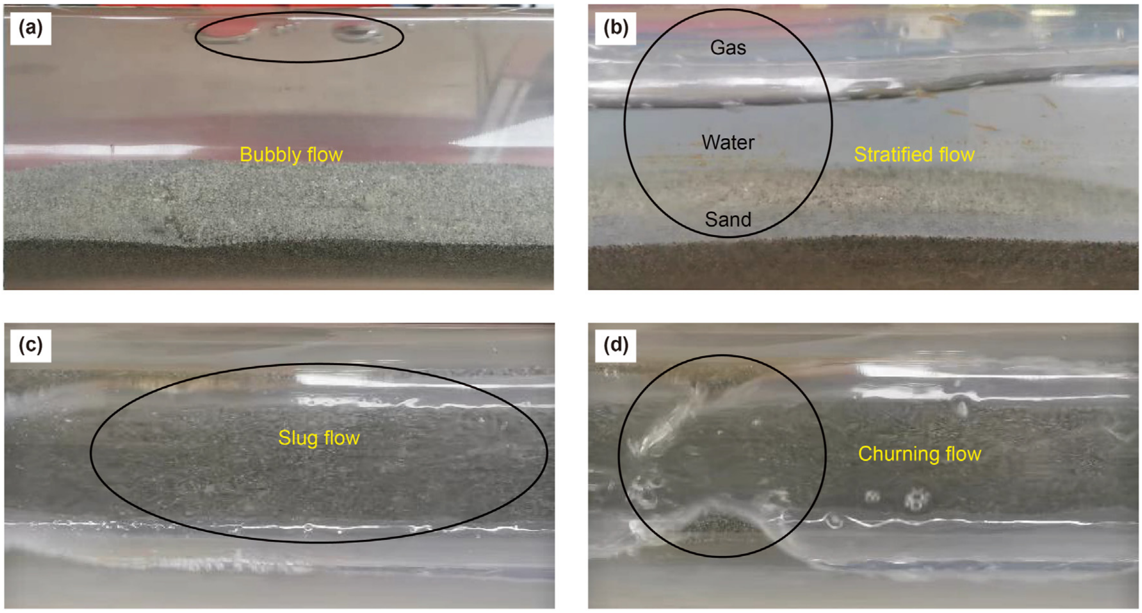

Fig. 4. Flow patterns at different gas void fractions: (**a**) 5%; (**b**) 20%; (**c**) 30%; (**d**) 50%. Other experiential conditions are as follows: hole deviation angle, 90°; sand particle diameter, 10 μm; sand concentration, 10%.

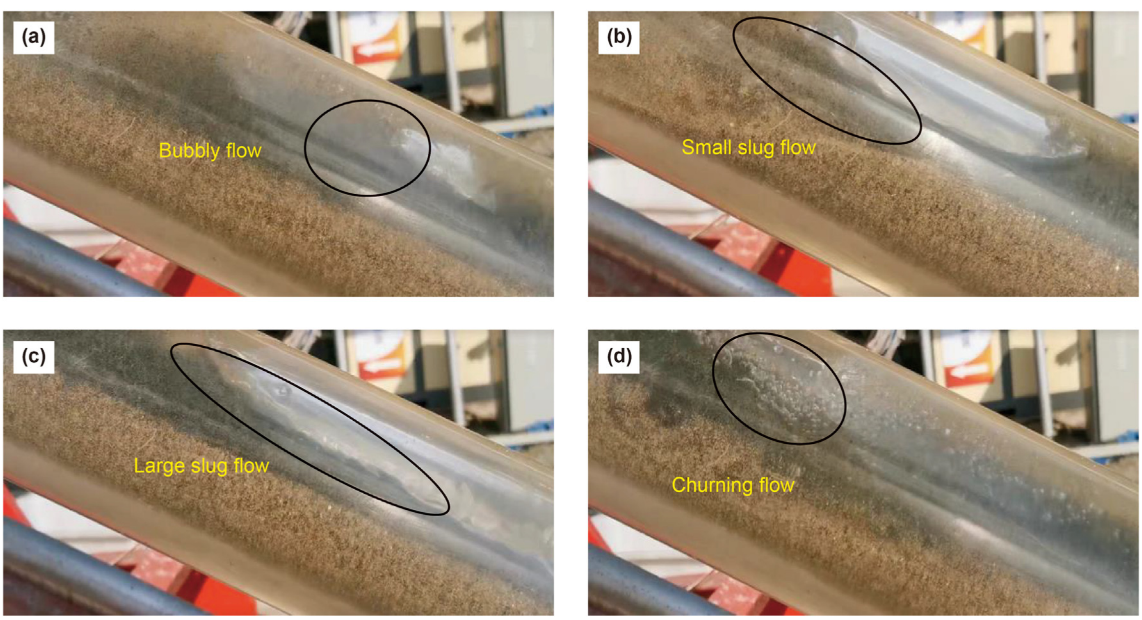

Fig. 5. Flow patterns at different gas void fractions: (**a**) 5%; (**b**) 20%; (**c**) 30%; (**d**) 50%. Other experiential conditions are as follows: hole deviation angle, 60°; sand particle diameter, 40 μm; sand concentration, 50%.

comprehensive analysis of the test results, while the gas void fraction and hole deviation angle made a great impact on it. Consequently, the pie chart of flow pattern based on different gas void fraction was drawn, as shown in Fig. 6.

When the gas void fraction was lower than 5%, the flow pattern was mainly bubbly flow. When it was between 5% and 10%, the bubbly flow was transformed as a coexistence state including bubbly flow and small slug flow. Under this circumstance, if the hole deviation angle was 90°, there was obvious stratified flow. Otherwise, there was no this kind of phenomenon. This is because the density of the gas, water and sand was different and the drag force of the fluid made little effect on the movement of sand particles under this condition.

When the gas void fraction increased from 10% to 30%, the small slug flow was transformed into a large slug flow, but there was still bubbly flow locally. When the gas void fraction was improved close to 50%, the large slug flow began to transform into agitated flow. When the gas void fraction was more than 50%, the flow pattern was altered to the agitated flow. Under this circumstance, if the hole deviation angle was 90° or less than 90°, the liquid flowed forward in a “wave shape” or in a “spiral shape”. This is because the drag force exerted on the sand particles was relatively small at 90°, so the stratified flow was main phenomenon. However, there were certain fluctuations due to the high gas void fraction, so the sand

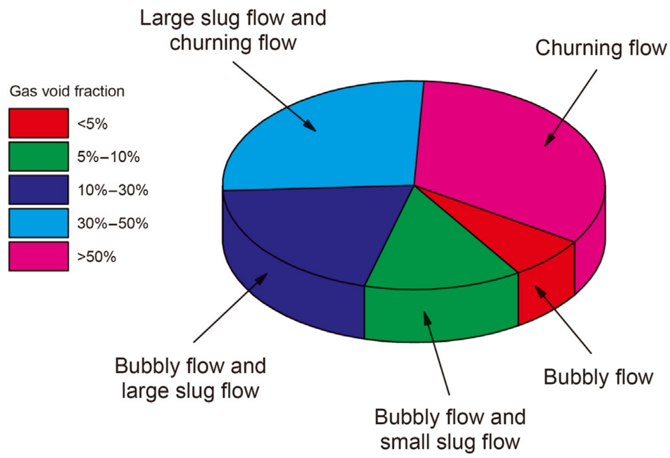

Fig. 6. Flow pattern of gas–water–sand three-phase flow based upon different gas void fractions.

bed appeared a wave-shaped. While the hole deviation angle was less than 90°, the drag force of the fluid exerted on the sand particles enlarged, which made the sand particles move forward more violently.

3.2. The phenomenon of sand migration

3.2.1. The effect of large slug flow on sand migration

Due to the similar rule of sand migration at other hole deviation angles, the analysis of the experimental results at hole deviation angles of 85° and 60° were taken as examples.

(1) Sand migration at the hole deviation angle of 85°

Before the large slug bubble passed through the pipe, the flow state was relatively stable and the surface sand bed moved forward as a whole (Fig. 7a1). Because the hole deviation angle was close to 90°, there was a layering phenomenon in the pipe. Moreover, the bubbles were mainly distributed in the upper layer of the pipe and the gas phase made limited influence on the flow state. The migration of sand particles mainly relied on the drag force of the liquid to achieve stable migration. Eventually, the phenomenon of overall migration of surface sand bed was observed.

In Fig. 7a2, the large slug bubble was just passing through. Because of the stratification phenomenon, the large slug bubble was distributed in the upper layer of the pipe and the surface sand bed slide down severely in the opposite direction of the fluid flow. The main reason was that a larger space in the pipe was occupied by the large slug bubble, which reduced the liquid content in the pipe. As a result, the drag force of the liquid exerted on the sand particles significantly reduced.

After the large slug bubble passed through the pipe, the fluid flow returned to a relatively stable state, as shown in Fig. 7a3. Similar to the situation in Fig. 7a1, the surface sand bed began to move stably along the direction of fluid flow.

(2) Sand migration at the hole deviation angle of 60°

Fig. 7b1 shows the sand migration before the large slug bubble passed. As the hole deviation angle reduced, the state of stratified flow weakened, the drag force of the gas exerted on the liquid enhanced. Once a bubbly flow occurred in the pipe, the surface sand bed migrated as a whole. When a small slug flow appeared, part of the sand particles moved forward in the form of tumbling and jumping. If it was the small slug flow, the drag force exerted on the liquid by the gas phase increased evidently. As a result, the gas carried the liquid and then the liquid also carried the sand particles, which made the sand particles move forward in the form of jumping and tumbling.

Fig. 7b2 shows the sand migration when the large slug bubble was passing through. Once the large slug flow appeared, the surface sand bed slid down in the opposite direction relative to fluid flow. As the gas void fraction was improved, a larger space in the pipe was occupied by the gas. On that account, the effect of the liquid made on the sand migration significantly weakened. Due to the decrease in hole deviation angle, the gravity exerted on the sand particles raised. Combining the above two effects, as the hole deviation angle and gas void fraction lifted, the phenomenon of sand falling was more conspicuous.

After the large slug bubble passed through the original area in the pipe, the falling sand particles at this area would violently collide with the fluid along the flow direction, as shown in Fig. 7b3. The obvious local turbulence and greater jumping migration appeared.

In summary, it was the phenomenon of overall migration of surface sand bed before a large slug bubble passed this space in an inclined pipe. When a large slug bubble has passed, the surface sand bed slid down in the opposite direction of the flow direction. As the hole deviation angle reduced, the sand bed was falling more evidently. After a large slug bubble passed, the surface sand bed reached the state of stable migration. Consequently, the large slug bubble was not conducive to sand migration.

3.2.2. The effects of gas void fraction on sand migration at different hole deviation angles

In Fig. 8a, the hole deviation angle was 90°, sand concentration was 20%, and gas void fraction was 5%. Because the test pipe was horizontal, the three phases of gas, water, and sand exhibited a very obvious phenomenon of stratified flow in the pipe. The gas, liquid, and sand separately distributed in the upper, middle and lower areas in the pipe. Under this circumstance, the gas void fraction was relatively small and the gas phase exerted rather small drag force on the liquid and sand bed. Therefore, the sand particles mainly moved forward by the drag force of the liquid. Finally, the overall migration of the surface sand bed was observed.

When the gas void fraction reached 10%, the drag force of the gas phase exerted on the liquid phase increased. In Fig. 8b, the hole deviation angle was 90°, sand concentration was still 20%, the pulsation of the gas phase of the upper area appeared in the pipe due to the increase in the gas void fraction and the flow of the liquid presented the "wave shape". What's more, the gas void fraction was low and the liquid content was high at the peak position of the wave flow, resulting in local accumulation of sand particles. At the trough position of the wave flow, the flow rate of the liquid was fast and the sand transport was easier due to the higher gas void fraction and lower liquid content. As a result, the sand bed showed a distribution of the wave-shaped.

Fig. 8c shows the state of steady flow after the wave distribution disappeared at the hole deviation angle of 90°, the sand concentration of 20%, and the gas void fraction of 20%. As the flow state was restored to stability, the similar phenomenon of stratified flow was shown in Fig. 8a. The regular wave-shaped distribution appeared due to the wave flow.

In Fig. 8b1, when the hole deviation angle was 85°, sand concentration was 20% and gas void fraction was 10%, the stratified flow disappeared due to the reduce of hole deviation angle. Furthermore, the flow pattern mainly consisted of small slug flow and bubbly flow. Because the gas void fraction was small (10%), the drag force exerted on the liquid and the sand particles was limited.

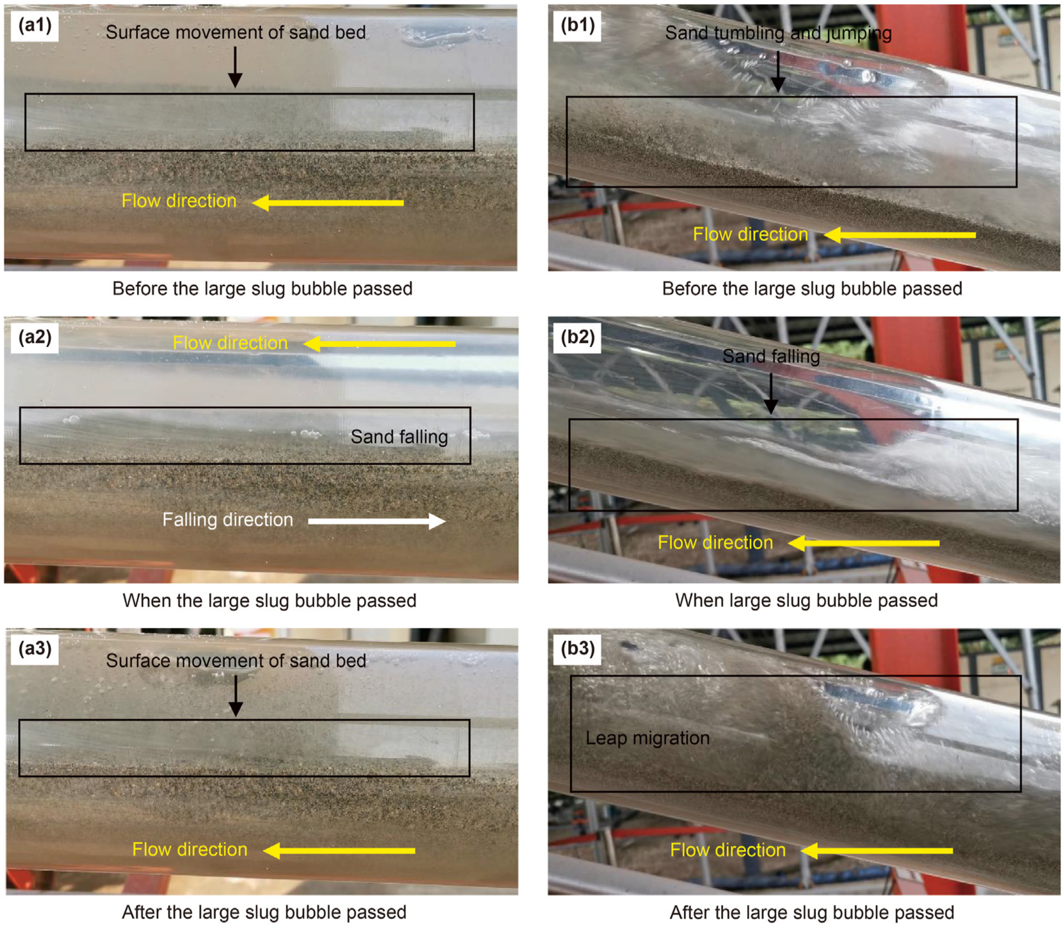

Fig. 7. The effect of large slug bubble on sand migration at different hole deviation angles: (**a1**, **a2**, **a3**) 85°; (**b1**, **b2**, **b3**) 60°.

The sand particles mainly relied on the drag force of the liquid to attain stable migration as well as the overall migration of the surface sand bed.

In Fig. 8b2, the hole deviation angle was 85°, sand concentration was 20%, and the gas void fraction was 20%. Compared with that in Fig. 8d, the turbulence state was more obvious because the due to the increase in the gas void fraction (from 10% to 20%). In addition, the higher gas void fraction improved the drag force of the gas phase on the sand particles, which made the surface sand bed roll and jump.

In Fig. 8c1, the hole deviation angle was 80°, the sand concentration was 30%, and the gas void fraction was 10%. Under this condition, the phenomenon of stratified flow disappeared. The flow pattern was mainly bubbly flow and small slug flow, which was similar to that in Fig. 8d.

In Fig. 8c2, the hole deviation angle was 80°, the sand concentration was 30%, and the gas void fraction was 20%. Because the gas void fraction was higher, the drag force of the gas phase exerted on the liquid and the sand particles was greater. As a result, the gas carried the liquid, and then the liquid further carried the sand, the occasion of the jumping and rolling of surface sand bed presented.

In Fig. 8d1, the hole deviation angle was 70°, the sand concentration was 30%, and the gas void fraction was 10%. As the inclination angle of the pipe was greater than that in Fig. 8f, the negative influence of gravity on sand migration was greater. The sand migration mainly relied on the drag force of the liquid to move forward, which was manifested as the overall migration of surface sand bed. Under this condition, the flow velocity of the liquid became obviously higher than that in former.

In Fig. 8d2, the hole deviation angle was 70°, sand concentration was 30% and gas void fraction was 20%. Because the gas void fraction was higher than that in Fig. 8h, the turbulence state in the pipe was more obvious. The sand particles were easier to be carried by the liquid due to the increase in the drag force of the gas exerted on the liquid. Therefore, the phenomenon of rolling and jumping of sand particles presented.

In Fig. 8d3, the hole deviation angle was 70°, the sand concentration was 30% and the gas void fraction was 30%. The turbulence in the pipe was more prominent than that in Fig. 8i due to the increase in gas void fraction. Consequently, the drag of the gas exerted on the liquid was further improved, which made it easier to carry sand particles. Finally, the violent spiral tumbling and jumping migration appeared.

In summary, when the hole deviation angle was 90° and the gas void fraction was lower than 5%, the flow pattern was mainly the stable stratified flow and the surface sand bed migrated as a whole. When the gas void fraction reached 10%, it was a wave flow and the sand particles migrated forward by the drag force of the liquid. Once the wave flow disappeared, a wavy sand bed formed. As the increase in the gas void fraction, the gas pulsation became more obvious, the small and large slug flow formed simultaneously. Finally, the overall migration of the surface sand bed formed based on the combined action of gas and liquid phases. When the hole deviation angle was less than 90°, the stratified flow in the pipe disappeared. Under this circumstance, the gas void fraction was less than 10%, it was mainly the overall migration of surface sand bed.

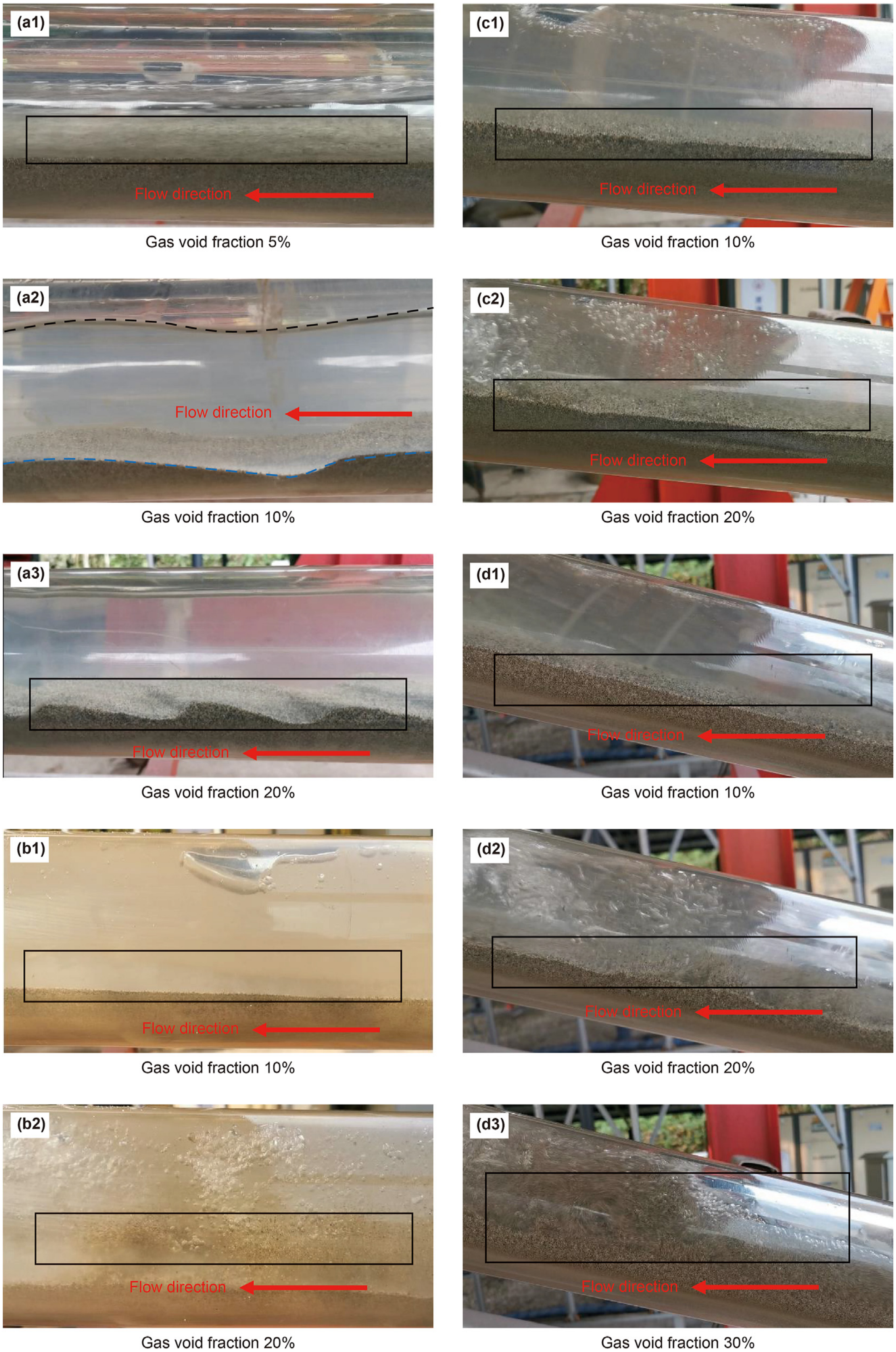

Fig. 8. The effects of gas void fraction on sand migration at different hole deviation angles and sand concentrations: (**a1**, **a2**, **a3**) hole deviation angle 90°, sand concentration 20%; (**b1**, **b2**) hole deviation angle of 85°, sand concentration 20%; (**c1**, **c2**) hole deviation angle 80°, sand concentration 30%; (**d1**, **d2**, **d3**) hole deviation angle 70°, sand concentration 30%.

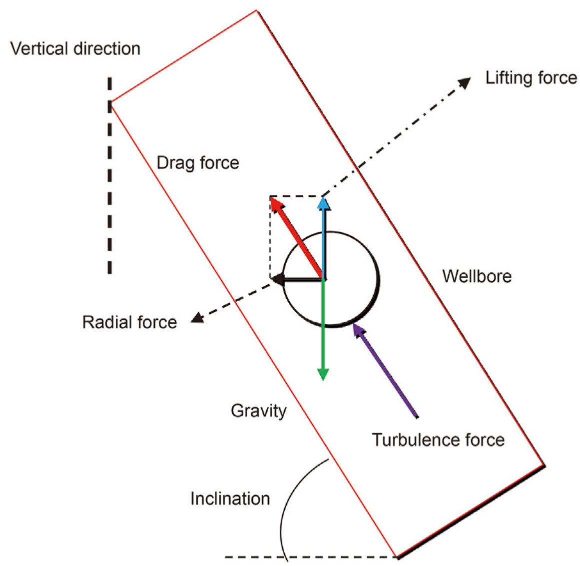

Fig. 9. Mechanical analysis of a single sand particle.

The gas void fraction reached 20%, the sand particles rolled and jumped. Once the gas void fraction reached 30%, the sand particles exhibited violent spiral tumbling and jumping migration.

3.3. Critical sand starting velocity

The forces on the sand particles during transport are mainly the drag force of the gas or liquid phase and the turbulence force of the fluid. The force analysis for a single sand in the tube is shown in Fig. 9. During sand migration, the driving force for forward migration is provided by the turbulent force and traction force, and gravity is the resistance. The drag force can be decomposed into vertical lift and horizontal radial force. The lift provided source of power for the upward migration of sand particles, while the radial force made the sand particles move along the inner wall of the pipe. Under gas–water–sand three-phase flow conditions, sand particles are transported forward by the combined action of the gas and liquid phases. The surface sand is instantaneously transformed from a completely stationary state to a forward migration state when the liquid flow velocity gradually increases. At this time, the liquid flow velocity is the critical sand starting velocity.

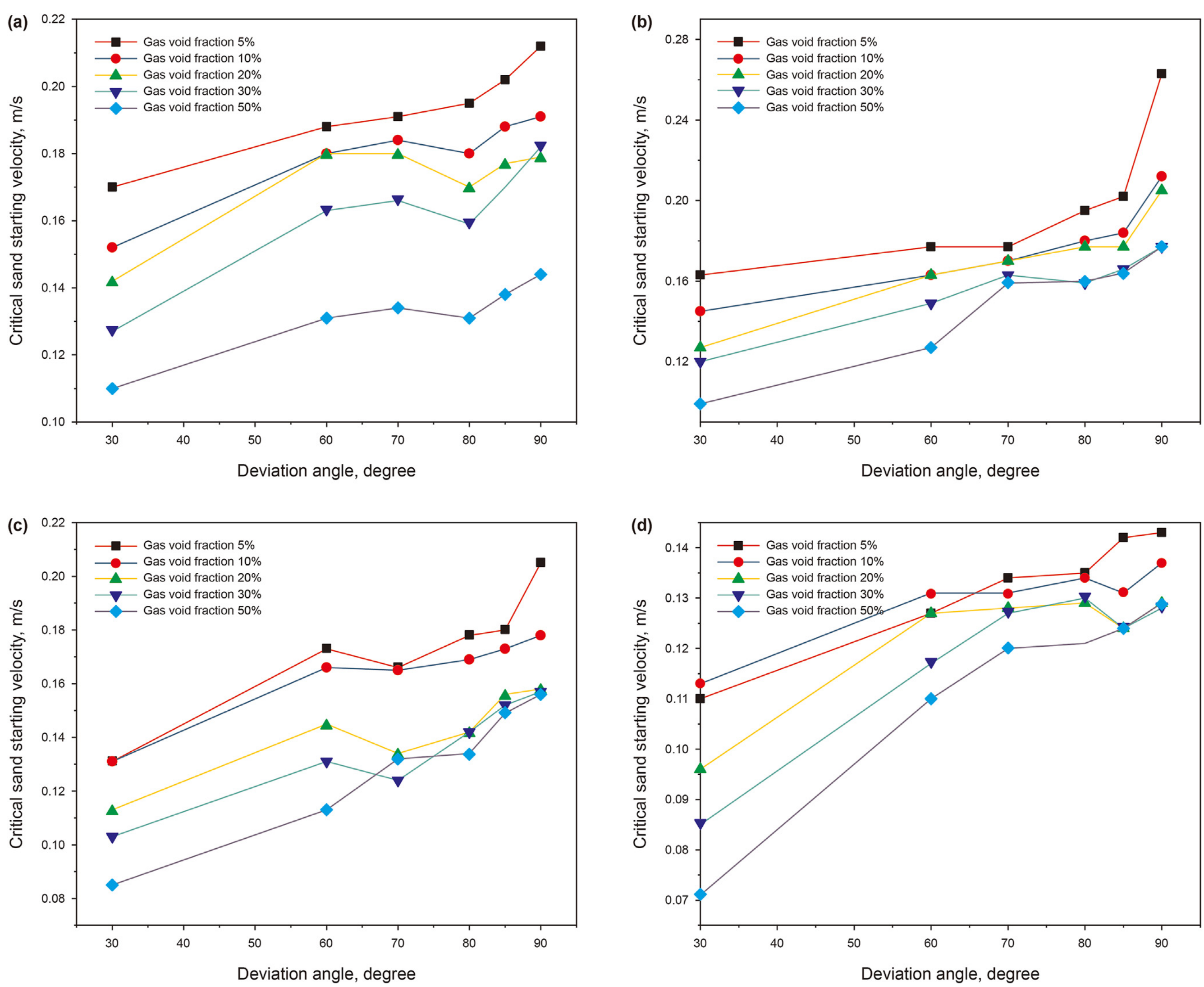

Fig. 10. The effect of hole deviation angle on the critical sand starting velocity at different sand concentrations: (**a**) 1%; (**b**) 10%; (**c**) 30%; (**d**) 50%.

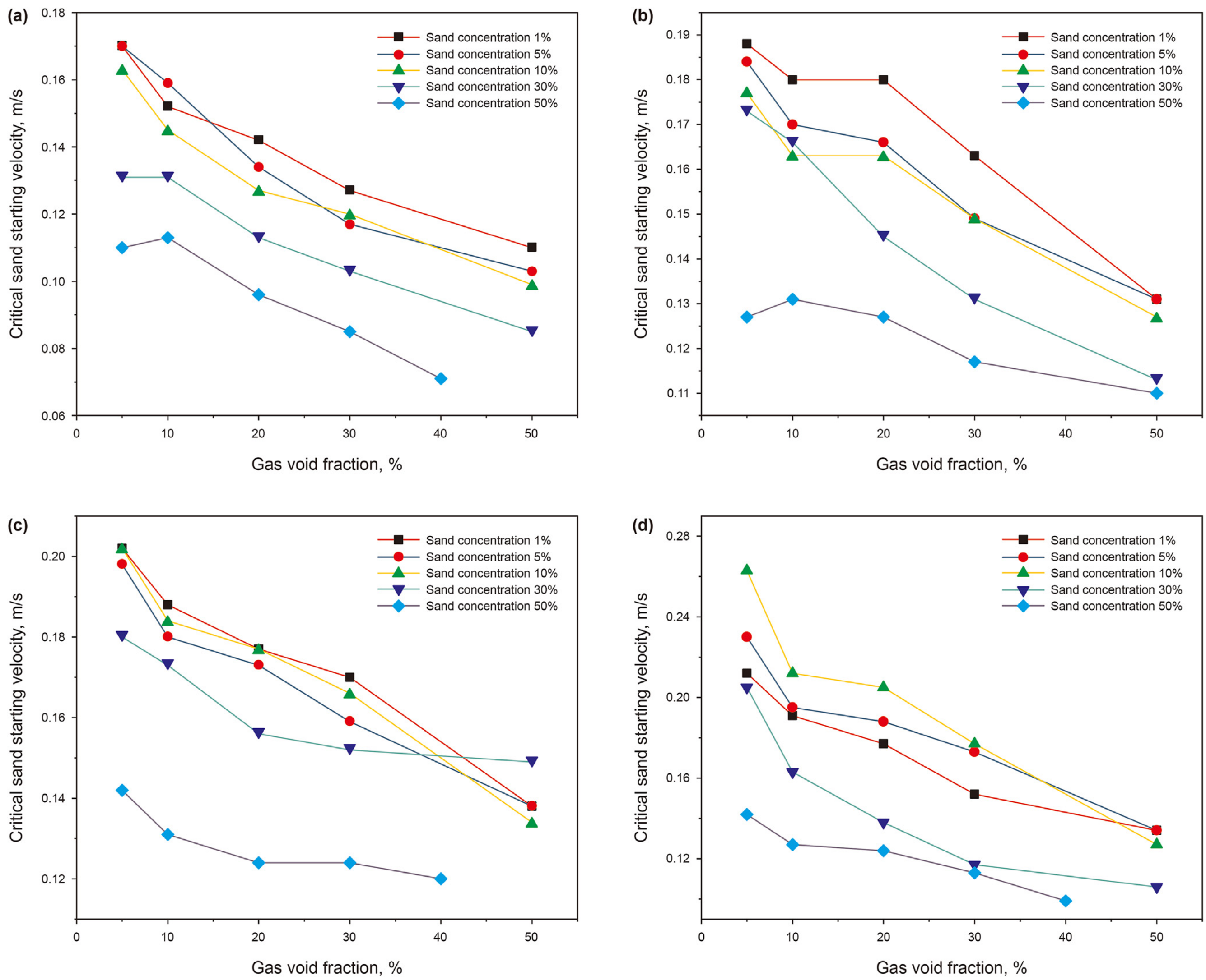

Fig. 11. The effect of gas void fraction on the critical sand starting velocity at different deviation angles: (**a**) 30°; (**b**) 60°; (**c**) 85°; (**d**) 90°.

3.3.1. The influence of hole deviation angle

When the sand concentration and gas void fraction kept constant, the critical sand starting velocity generally presented an increasing trend with the rise of hole deviation angle, as shown in Fig. 10. As the hole deviation angle raised, the reduce of lifting force and the increase of the radial force made it more difficult to carry sand particles. Deposition in the pipe was easier to form. During conventional drilling, it is the most difficult for sand particles to migrate effectively at the hole deviation angle of 45°–60° rather than the other deviation angle, which results in forming the most serious sand bed deposition. The micron-scale sand used for dual-gradient drilling based on double-layer pipe is easier to deposit on the wellbore. The smaller the sand particle size is, the larger the specific surface area and the stronger adhesion between the sand and the wellbore will be. The larger the hole deviation angle was, the greater adhesion between the sand and the wellbore will be, and the critical sand starting velocity was higher. When the hole deviation angle reached 80° or more, the three phases of gas, water, and sand began to show obvious stratified flow. The gas, liquid and sand were separately located in the uppermost layer, the middle layer and the lower layer in the pipe. Providing that the hole deviation angle further raised, the turbulence state in the pipe weakened and the turbulence force decreased, which made the critical sand starting velocity increase.

3.3.2. The effect of gas void fraction

It can be seen from Fig. 11, when the hole deviation angle and sand concentration was constant, the critical sand starting velocity generally presented a decreasing trend with the increase in gas void fraction. On the one hand, the turbulence state was more obvious due to the increase in gas void fraction, which resulted in the turbulent force augmenting. As the turbulence intensity increased, the flow rate and the lift force of the liquid phase relative to the sand particles also increased. The pressure difference between the upper and lower space of the sand bed increased with the growth of liquid flow rate, so the lifting force became greater. On the other hand, the drag force of the gas exerted on the liquid was greater due to the higher gas void fraction. The greater drag force made it easier for sand particles to migrate, resulting in the gradual reduce of the critical sand starting velocity.

3.3.3. The effect of sand concentration

It can be seen from Fig. 12, the critical sand starting velocity generally showed a decreasing trend with the increase in sand

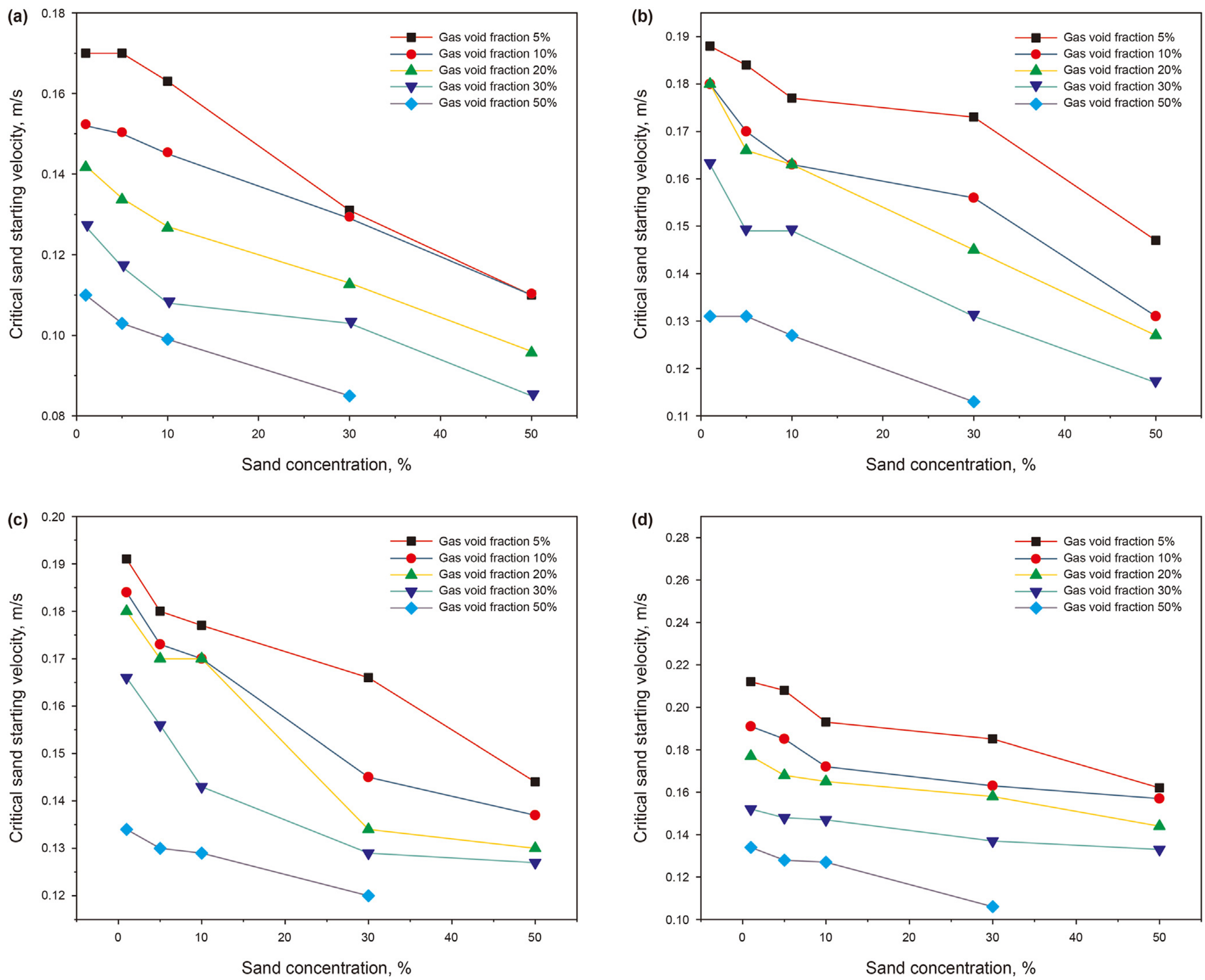

Fig. 12. The effect of sand concentration on the critical sand starting velocity at different deviation angles: (**a**) 30°; (**b**) 60°; (**c**) 85°; (**d**) 90°.

concentration when the hole deviation angle and the gas void fraction kept constant. Because the sand concentration became higher, the cross-sectional area occupied by the fluid was smaller and the flow rate of the fluid will be greater. Providing that the gas void fraction and fluid flow rate were constant, the drag force exerted on the sand particles enhanced dramatically as the sand concentration increased. Therefore, it was more conducive to the sand particles to migrate, which further made the critical sand starting velocity decrease.

3.3.4. The effect of sand diameter

It can be seen from Fig. 13, the critical sand starting velocity was positive correlation with the particle size. When the gas void fraction and sand concentration remained constant, the drag force exerted on the sand particle was basically the same. On the one hand, the gravity exerted on the sand particle enhanced significantly due to the larger particle size and the greater difficulty of sand migration. On the other hand, its specific surface area became smaller as the particle size was larger. So, the sand particle was difficult to suspend or carried by the liquid phase. Hence the critical sand starting velocity increased along with the growth of sand particle size.

3.3.5. Dimensionless analysis

According to the above experimental results, it can be seen that the critical sand starting velocity is comprehensively affected by multiple factors, such as the hole deviation angle, gas void fraction, sand particle size, and sand concentration. It is not possible to directly compare the influence degree made by different factors on the critical sand starting velocity. Consequently, it is necessary to utilize the dimensionless analysis method to carry out dimensionless processing of the four influencing factors. Finally, the influence degree of each factor can be compared based on the dimensionless results.

Weighting method of the coefficient of variance was introduced in this paper to deal with the different influencing factors. Then the comprehensive index of different influencing factors was compared to judge the degree of influence. The larger the comprehensive index is, the greater the degree of influence will be.

Firstly, the influencing factors in the experiment, such as deviation angle, gas void fraction, sand concentration and diameter of the sand were defined as different indexes. Then the data matrix of the critical sand starting velocity based upon different indexes were non-dimensionalized. Therefore, the standardized matrix $\Gamma = (\boldsymbol{R}_{ij})_{m\times n}$ under the corresponding conditions was obtained, as

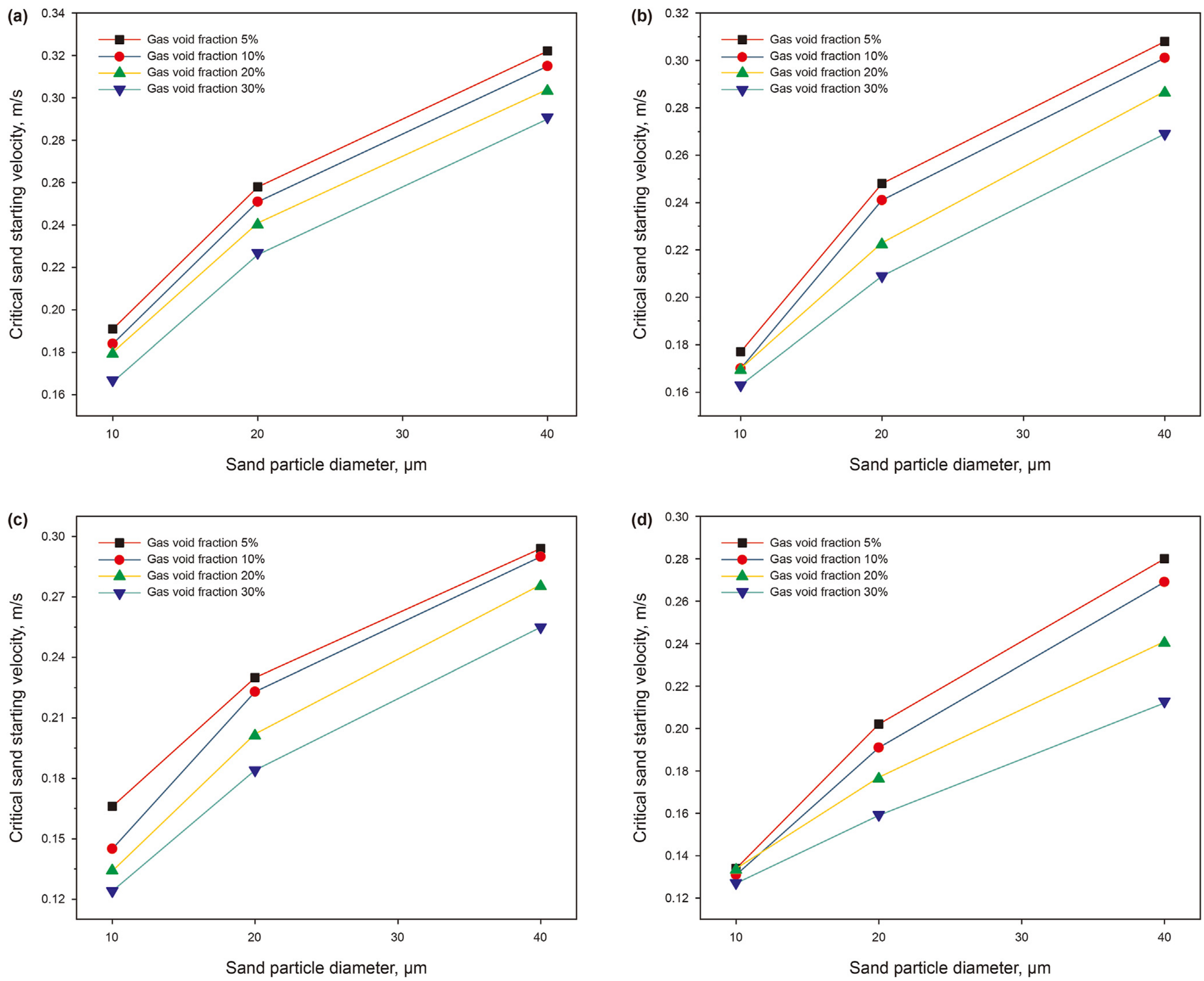

Fig. 13. The effect of sand particle diameter on the critical sand starting velocity at different sand concentrations: (**a**) 1%; (**b**) 10%; (**c**) 30%; (**d**) 50%.

shown in Eq. (1).

$$\boldsymbol{R}_{ij} = \frac{x_{ij}}{x_j} \tag{1}$$

where j is the deviation angle, gas void fraction, sand concentration and diameter of sand.

The standard deviation and the average value under the above-mentioned different index conditions from the standardized matrix $\Gamma = (\boldsymbol{R}_{ij})_{m \times n}$ can be obtained. Further, the coefficient of variation of different indexes was calculated according to the standard deviation and the average value, as shown in Eq. (2).

$$\chi_j = \frac{\sigma_j}{\mu_j} \tag{2}$$

where χ_j is the coefficient of variance of the index j, also known as the standard deviation coefficient; σ_j is the standard deviation of the index j; μ_j is the average of the index j.

The coefficients of variance of different indexes can be obtained by Eq. (2), and then the weights of different indexes can be calculated by Eq. (3).

$$W_j = \frac{\chi_j}{\sum\limits_{j=1}^{n} \chi_j} \tag{3}$$

where W_j is the weight for the index j.

The above calculations only get the weighting results under different index conditions, but the impact on the evaluation results caused by the difference in dimensions between different index has not been eliminated.

Therefore, in order to eliminate the influence of the dimension between the index, the normalization formula of root mean square error was utilized in this paper, as shown in Eq. (4), to normalize the different indexes, and unified their values in the interval [0, 1]. The normalized value was closer to 1, the greater the degree of influence will be, and vice versa, the smaller the degree of influence will be.

$$\ell = \frac{\lambda_j - \min(\lambda_j)}{\max(\lambda_j) - \min(\lambda_j)} \tag{4}$$

where ℓ is the normalized value of the root mean square error of

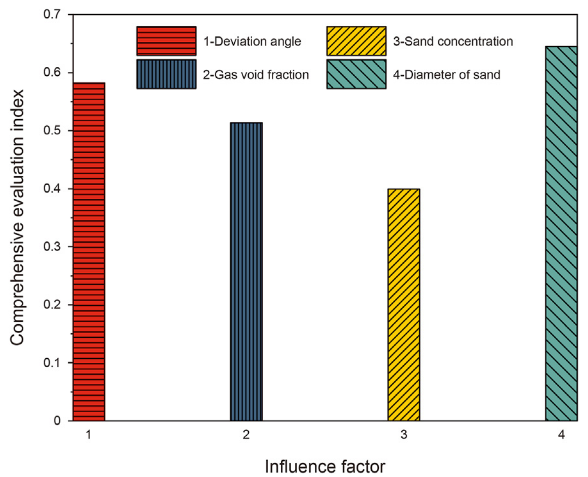

Fig. 14. Comparison of the influence of different factors on the critical sand starting velocity.

different indexes; λ_j is the root mean square error of the index j.

Finally, Eqs. (3) and (4) were combined to obtain the comprehensive evaluation index I that eliminated the influence of dimensions. The closer the value of the comprehensive evaluation index was to 1, the greater the degree of influence of the index will be.

$$I = \sum W_j \ell = \sum \left(\frac{\chi_j}{\sum_{j=1}^{n} \chi_j} \frac{\lambda_j - \min(\lambda_j)}{\max(\lambda_j) - \min(\lambda_j)} \right) \tag{5}$$

where I is a dimensionless comprehensive evaluation index.

According to Eq. (5), the values of comprehensive evaluation indexes under different well deviation angle, gas void fraction, sand concentration and sand diameter were calculated, as shown in Fig. 14. It can be seen that the values of the comprehensive evaluation indexes of sand diameter, deviation angle, gas void fraction and sand concentration decreased successively, so the degree of their influence on the critical sand starting velocity gradually decreased in order.

4. Conclusions

The transformation rule of flow pattern based on different gas void fractions, and the critical sand starting velocity of gas–water–sand three-phase flow under the conditions of different hole deviation angle, gas void fraction, sand particle size and sand concentration in the inclined pipe were studied by laboratory experiment. In a addition, the influence of large slug bubble on the migration of sand bed was studied. Finally, weighting method of the coefficient of variance was utilized to compare and analyze the degree of influence of the deviation angle, gas void fraction, sand concentration and sand particles size on the critical sand starting velocity. Then the following conclusions were obtained.

(1) During the gas–water–sand three-phase flow, when the gas volume fraction is 5%, 5%–30%, or 30%–50%, the flow patterns are separately the bubbly flow, the transition of bubbly flow to slug flow and the transition of slug flow to agitated flow, respectively. During the transition state from bubbly flow to the slug flow, if the hole deviation angle is 90°, there will be obvious stratified flow.

(2) When the hole deviation angle is 90°, the gas void fraction is lower than 5%, the surface sand bed will migrate as a whole. If the gas void fraction is between 5% and 10%, the wavy sand bed appears in the pipe. Providing that the gas void fraction is greater than 10%, a small or large slug flow will appear, and the surface sand bed will migrate forward as a whole.

(3) When the hole deviation angle is less than 90°, the gas void fraction is less than 10%, the surface sand bed migrates forward as a whole. As the gas void fraction increases, rolling and jumping migration will be observed. The greater the gas void fraction is, the more significant the phenomenon will be. If the gas void fraction is more than 10%, it is beneficial for smooth migration. Nevertheless, the large slug bubble appearing intermittently exerts a negative impact on the effective migration of the sand bed in the inclined pipe.

(4) The critical sand starting velocity was positively related with the hole deviation angle and sand particle size, and negatively related with gas void fraction and sand concentration in inclined pipe. In addition, the influence degree of sand particle size, deviation angle, gas void fraction and sand concentration on the critical sand starting velocity decreases in order.

Acknowledgments

This work is supporting by the Youth Program of National Natural Science Foundation of China (52104012), the China Postdoctoral Science Foundation (2021M693494), the Key Program of the National Natural Science Foundation of China (51734010), the Key Natural Science Projects of Scientific Research Plan in Colleges and Universities of Xinjiang Uygur Autonomous Region (XJEDU2021I028), and the Strategic Cooperation Technology Projects of CNPC and CUPB (ZLZX2020-01-01).

References

Bello, K., Oyeneyin, B., 2016. Experimental investigation of sand minimum transport velocity in multiphase fluid flow in pipes. Niger. J. Technol. 35, 531–536. https://doi.org/10.4314/njt.v35i3.9.

Bhandari, J., Abbassi, R., Garaniya, V., Khan, F., 2015. Risk analysis of deepwater drilling operations using Bayesian network. J Loss Prevent Proc 38, 11–23. https://doi.org/10.1016/j.jlp.2015.08.004.

Chen, D., Pan, Z., Liu, J., 2012. Characteristic of anisotropic coal permeability and its impact on optimal design of multi-lateral well for coal bed methane production. J. Petrol. Sci. Eng. 88/89, 13–28. https://doi.org/10.1016/j.petrol.2012.04.003.

Dabirian, R., Kouba, G., Mohan, R.S., Shoham, O., 2016. Sand Flow Regimes in Slightly Upward Inclined Gas-Liquid Stratified Flow. ASME Fluid Engineering Division Summer Meeting.

Davies, J.T., 1987. Calculation of critical velocities to maintain solids in suspension in horizontal pipes. Chem. Eng. Sci. 42, 1667–1670. https://doi.org/10.1016/0009-2509(87)80171-9.

Dong, C., Luan, W., Zhou, S., et al., 2007. Analysis and application of solid particle motion model in Newtonian fluid. J. China Univ. Petrol. 31 (5), 55–59. https://doi.org/10.3321/j.issn:1000-5870.2007.05.012 (in Chinese).

Dong, C., Li, Y., Zhang, Q., et al., 2014. Experimental study on sand starting mechanism and capacity e-valuation in water producing gas wells and its application in artificial lift optimization. In: SPE Middle East Artificial Lift Conference and Exhibition. https://doi.org/10.2118/173700-MS.

Elgaddafi, R., Ahmed, R., George, M., Growcock, F., 2012. Settling behavior of spherical particles in fiber-containing drilling fluids. J. Petrol. Sci. Eng. 84–85, 20–28. https://doi.org/10.1016/j.petrol.2012.01.020.

GhasemiKafrudi, E., Hashemabadi, S.H., 2016. Numerical study on cuttings transport in vertical wells with eccentric drillpipe. J. Petrol. Sci. Eng. 140, 85–96. https://doi.org/10.1016/j.petrol.2015.12.026.

Gillies, R.G., McKibben, M.J., Shook, C.A., 1997. Pipeline flow of gas, liquid and sand mixtures at low velocities. J. Can. Pet. Tech. 36, 36–42. https://doi.org/10.2118/97-09-03.

Goharzadeh, A., Rodgers, P., 2009. Experimental characterization of solid particle transport by slug flow using particle image velocimetry. In: International Symposium on Measurement Techniques for Multiphase Flows. https://doi.org/10.1088/1742-6596/147/1/012069.

Guo, X.L., Wang, Z.M., Long, Z.H., 2010. Study on three-layer unsteady model of cuttings transport for extended-reach well. J. Petrol. Sci. Eng. 73 (1–2), 171–180. https://doi.org/10.1016/j.petrol.2010.05.020.

Jiao, Y., Deng, J., Mou, S., 2010. Calculation of the minimum sand starting speed in vertical wellbore s-and production. Western Exploration Eng. 22 (3), 101–103. https://doi.org/10.7623/syxb201805012 (in Chinese).

Keskin, C., Zhang, H., 2007. Identification and classification of new three-phase gas/oil/water flow patterns. In: SPE Annual Technical Conference and Exhibition. https://doi.org/10.2118/110221-MS.

Khan, N.U., May, R.A., 2016. Generalized mathematical model to predict transient bottomhole temperature during drilling operation. J. Pet. Sci. Eng. 147, 435–450. https://doi.org/10.1016/j.petrol.2016.08.017.

Li, G., Tian, S., Zhang, Y., 2020. Research progress on key technologies of cavitation jet drilling radial wells for natural gas hydrate production. Petrol. Sci. Bull. 5 (3), 349–365. https://doi.org/10.3969/j.issn.2096-1693.2020.03.030 (in Chinese).

Li, M., 2000. Sand-starting law of vertical wellbore. J. Univ. Pet. (China) 24 (2), 33–35. https://doi.org/10.3321/j.issn:1000-5870.2000.02.010 (in Chinese).

Lin, R., Shao, C., Li, J., 2013. Study on two-phase flow and heat transfer in offshore wells. J. Pet. Sci. Eng. 111, 42–49. https://doi.org/10.1016/j.petrol.2013.09.012.

Liu, A., Deng, J., 2007. Research on the minimum sand-starting velocity of low-viscosity liquid flow in vertical wells. Petrol. Drill. Product. Technol. 29 (1), 31–33 https://doi.org/JournalArticle/5aea376ec095d713d8a50c8b. (in Chinese).

Ma, Y., Sun, B., Shao, R., et al., 2014. Annular temperature of riser in double-gradient drilling with gas injection method Field simulation. Acta Pet. Sin. 35 (4), 779–785. https://doi.org/10.1016/10.7623/syxb201404022 (in Chinese).

Mutahar, F., 2006. Modeling of Critical Deposition Velocity of Sand in Horizontal and Inclined Pipes. MSc Thesis. The University of Tulsa, Tulsa.

Scott, D.S., Rao, P.K., 1971. Transport of solids by gas-liquid mixtures in horizontal pipes. Can. J. Chem. Eng. 49, 302–309. https://doi.org/10.1002/cjce.5450490302.

Shen, Y., Mao, J., Ling, S., 1999. The minimum rising water velocity of solid-liquid two-phase flow in vertical pipes. J. Univ. Sci. Technol. Beijing 21 (6), 519–522. https://doi.org/10.3321/j.issn:1001-053X.1999.06.003 (in Chinese).

Stevenson, P., Thorpe, R.B., 2003. Energy dissipation at the slug nose and the modeling of solids transport in intermittent flow. J. Can. Chem. Eng. 81, 271–278. https://doi.org/10.1002/cjce.5450810213.

Sui, B., Liu, G., Li, B., et al., 2016. The deposition and migration of particles in the fluctuating product oil pipeline. Acta Pet. Sin. 37 (4), 523–530. https://doi.org/10.7623/syxb201604012 (in Chinese).

Sun, X., Sun, B., Zhang, S., Wang, Z., Gao, Y., Li, H., 2018. A new pattern recognition model for gas kick diagnosis in deepwater drilling. J. Pet. Sci. Eng. 167, 418–425. https://doi.org/10.1016/j.petrol.2018.04.035.

Wang, G., Zhong, L., Liu, Q., Zhou, S., 2019. Research on deep-sea oil and gas and hydrate development technology based on double-layer pipes and double gradients. Mar. Eng. Equip. Technol. 6 (S1), 225–233 https://doi.org/CNKI:SUN:HYZB.0.2019-S1-044. (in Chinese).

Xin, X., Wang, H., Luo, J., Yu, H., Yuan, Y., Xia, Y., Zhu, H., Chen, Q., 2020. Simulation of depressurization production of marine gas hydrate horizontal wells based on machine learning method—optimized coupling model. Nat. Gas. Ind. 40, 149–158, 08, https://doi.org/CNKI:SUN:TRQG.0.2020-08-018. (in Chinese).

Zhang, G., Huang, X., Yan, J., Yin, L., Wang, W., Qu, X., Sun, X., 2001. Minimum sand-starting and lifting capacity of oil wells in Gudong Oilfield Research. J. Jianghan Petrol. Inst. 33–23 (3), 33–35+5-4. https://doi.org/CNKI:SUN:JHSX.0.2001-03-009. (in Chinese).

Zhang, Z., 2013. Research on the Gas-Liquid-Solid Flow Mechanism and the Liquid-Starting and Sand-Starting Capacity of Gas Wellbore. Ph.D. Dissertation. Qingdao: China University of Petroleum, East China (in Chinese).